High-visibility in-line fiber-optic optofluidic Fabry–Pérot cavity
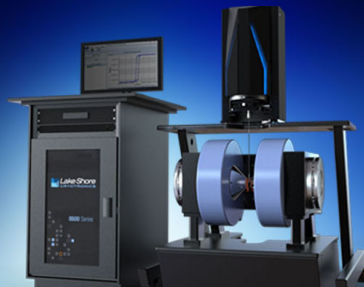
Qiang Zhang, Pengli Hao, Xinzhang Tian, and Yongmin Li

High-visibility in-line fiber-optic optofluidic Fabry–Pérot cavity

Qiang Zhang,[1,2,b)] Pengli Hao,[1] Xinzhang Tian,[1] and Yongmin Li[1,2,a)]
[1]*State Key Laboratory of Quantum Optics and Quantum Optics Devices, Institute of Opto-Electronics,*
Shanxi University, Taiyuan 030006, China
[2]*Collaborative Innovation Center of Extreme Optics, Shanxi University, Taiyuan 030006, China*

A high-visibility in-line optofluidic Fabry–Pérot (HVILOFFP) cavity was demonstrated by splicing a silica capillary tube into two standard single mode fibers (SMFs) and polishing the latter SMF. Two size-controllable microfluidic accesses in the sides of the HVILOFFP cavity allow the analyte of interest to smoothly flow into the cavity and directly interact with light without any assisting equipment to direct the analyte into the cavity. Experimental results showed that the fringe visibility of the HVILOFFP cavity was up to 24 dB in both air and water, which is higher than that of most laser-machined in-line fiber-optic Fabry–Pérot cavities because of the smoother end faces of the SMFs. The proposed HVILOFFP cavity was demonstrated by measuring the refractive indices with a sensitivity of 1148.93 nm/RIU in the range of 1.333–1.345. Moreover, the proposed HVILOFFP cavity is economical, compact ($<100 \, \mu$m), robust, and insensitive to temperature. These advantages make it a promising optofluidic platform in biomedical and chemical sensing applications. *Published by AIP Publishing.* https://doi.org/10.1063/1.4995296

Optofluidics combining photonics and microfluidics has been utilized in various exciting applications[1–4] due to its advantages of confining light and fluids in a small geometry to obtain a strong light-fluid interaction and monitoring the interaction in real time. Most traditional optofluidic sensing platforms are constructed on on-chip planar waveguides with microchannels and other off-chip optical devices. To achieve miniaturized robust optofluidic platforms for practical applications, a number of approaches based on optical fibers have been proposed because optical fibers have the distinct advantages of small size, robustness, easy light coupling, low transmission loss, and telemetry. A common approach is to employ microstructured optical fibers (MOFs) as optofluidic platforms.[5–13] The analyte of interest is injected into the air holes of the MOF, and it interacts with light in the core of the MOF. In this approach, a long interaction length between the analyte and light can be realized easily to enhance the sensitivity of optofluidic systems. Special accesses should be designed to replace and manipulate the analyte flexibly in the air holes of the MOF, such as by drilling holes in the side of MOF[7,8] and using a C-shaped fiber[9] or a side-polished single mode fiber (SMF).[10] Another promising approach is to use Fabry–Pérot (FP) cavities with microfluidic accesses.[14–22] The FP cavities can be formed by using cantilevers[4,14,15] and suspended-core fibers[16] and directly fabricating an SMF by using a femtosecond laser[17–19] and a focused-ion beam[20,21] or via photolithography.[22] The optofluidic FP cavities used in this approach provide potential accesses to analyte samples for direct interactions with light in the FP cavities. Moreover, the use of an interferometer increases the sensitivity of optofluidic devices. However, the surface machined by the laser and the focused-ion beam is usually rough and needs to be smoothed further by some special methods, and the micromachining equipment

is expensive. The suspended-core fiber with fixed microstructures limits the design flexibility of the devices.

In this letter, we demonstrate a high-visibility in-line optofluidic Fabry-Pérot (HVILOFFP) cavity based on a silica capillary tube (SCT) and SMF. The end faces of the SMFs form an optical FP cavity. Two size-controllable microfluidic accesses are fabricated in the sides of the FP cavity by polishing the latter SMF with a suitable inclination. This arrangement ensures that different analyte fluids can smoothly access the HVILOFFP cavity and interact with light without any auxiliary equipment to direct the fluids into the cavity. Moreover, the fringe visibility of the HVILOFFP cavity is higher than that of most laser-machined in-line fiber-optic FP cavities because the end faces of the SMFs cleaved using a fiber cleaver are smoother than those fabricated by using a laser. Experimental results showed that the fringe visibility of the HVILOFFP cavity was up to 24 dB both in air and in water. Furthermore, the economical raw materials and simple fabrication process make the proposed device extremely low-cost. Therefore, the HVILOFFP cavity is a promising optofluidic platform in chemical and biomedical sensing applications.

The fabrication process of the HVILOFFP cavity is relatively straightforward and is shown in Figs. 1(a)–1(d). First, the end faces of two SMFs and an SCT are cleaved by using an optical fiber cleaver (S326, FITEL). Second, the cleaved end face of the SCT is spliced into one of the SMFs using a fusion splicer machine (S183 ver. 2, FITEL), with an arc power of 70, a fusion time of 0.12 s, and a push distance of $10 \, \mu$m. Third, as shown in Fig. 1(a), the SCT with length L_1 is cleaved, and the other part is removed, which can be performed with more accuracy under a microscope with a CCD camera. Then, the cleaved end face of the SCT is spliced to the other SMF as shown in Fig. 1(b), where an in-line fiber-optic FP cavity with cavity length L_1 is formed by the end faces of the two SMFs. Further, as shown in Figs. 1(b) and 1(c), the latter SMF with length L_2 is cleaved and roughened

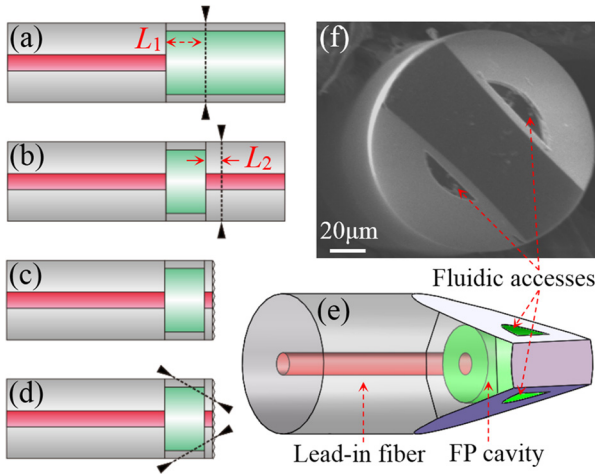a)yongmin@sxu.edu.cn.
b)qzhang@sxu.edu.cn.

FIG. 1. (a)–(d) Schematic of the fabrication process of the HVILOFFP cavity, (e) 3D model schematic of the HVILOFFP cavity, and (f) SEM image of the cavity with $L_1 = 94\,\mu m$ and $L_2 = 5\,\mu m$.

by using a fiber-end polisher with a 3-μm-diameter-grain abrasive film to eliminate the light reflected by the other end face of the latter SMF. Subsequently, as shown in Fig. 1(d), microfluidic accesses can be fabricated by polishing the latter SMF with a fiber-end polisher (krelltech, the inclination accuracy is 0.04°), where the size of the microfluidic access can be tailored flexibly by controlling the polishing inclination and length. A 3D model schematic of the HVILOFFP cavity is shown in Fig. 1(e). Figure 1(f) shows a scanning electron microscopy (SEM) image of the cavity, where the sizes of the two microfluidic accesses are 40 and 46 μm, respectively. The accesses are polished with 50° inclination and 40 and 45 μm polishing lengths. In our experiments, the SCT with an inner diameter of 70 μm and an outer diameter of 125 μm was purchased from BEIJING XING-YUAN-AO-TE OPTOELECTRONIC TECH. Co., LTD.

The operating principle of the HVILOFFP cavity is illustrated in Fig. 2. Light emanating from a broadband source (BBS) with a wavelength in the range of 1520–1620 nm was coupled into the HVILOFFP cavity through a circulator, and the reflection spectrum from the HVILOFFP cavity was monitored using an optical spectrum analyzer (OSA203, Thorlabs). The light beams reflected by the two end faces of the SMFs superimpose to generate a two-beam FP interference signal. The normalized reflection spectrum $I_{FP}(\lambda)$ of the HVILOFFP cavity can be given as
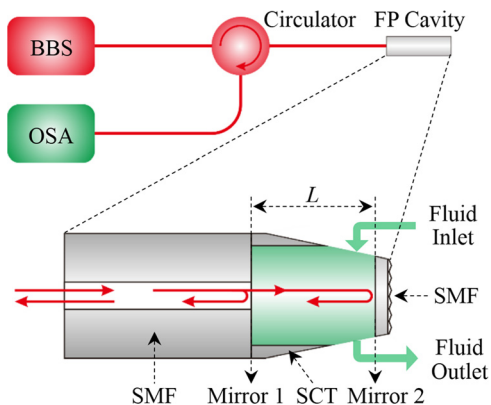

FIG. 2. Schematics of the experimental setup and the HVILOFFP cavity.

$$I_{FP} = R_1 + (1 - \alpha_1)^2 (1 - \alpha_2)(1 - \gamma)^2 (1 - R_1)^2 R_2$$
$$+ 2\sqrt{R_1 R_2 (1 - \alpha_2)}(1 - \alpha_1)(1 - \gamma)(1 - R_1)$$
$$\times \cos\left(4\pi n_{an} L / \lambda + \pi\right), \tag{1}$$

$$R_1 = R_2 = (n_{co} - n_{an})^2 / (n_{co} + n_{an})^2, \tag{2}$$

$$\gamma = \gamma_1 + \gamma_2, \tag{3}$$

$$\gamma_2 = kL / n_{an}, \tag{4}$$

where R_1 and R_2 are the light reflection coefficients at the end faces of the SMFs, α_1 *and* α_2 are the attenuation factors of the light intensity at Mirrors 1 and 2 due to the imperfect end faces of the SMFs (e.g., roughness), L is the length of the cavity, λ is the wavelength of the input light, n_{an} and n_{co} are the refractive indexes (RIs) of the analyte fluid and optical fiber, respectively, π is from the half-wave loss at Mirror 1 ($n_{an} > n_{co}$) or Mirror 2 ($n_{an} < n_{co}$), k is a constant, and γ is the transmission loss factor of the FP interferometer, which consists of the absorption loss γ_1 from the fluid in the cavity and the mode-mismatch loss γ_2 between the former SMF and the light reflected by the latter SMF.

The free spectrum range (FSR), which is the distance between two adjacent dip intensities in the reflection spectrum, can be expressed as

$$FSR = \lambda^2 / 2n_{an} L. \tag{5}$$

In the destructive interference reflective spectrum of the FP cavity, the dip wavelength λ_m is given by

$$\lambda_m = 2L n_{an} / m. \tag{6}$$

Therefore, we can measure the RI of the analyte in the FP cavity by monitoring the shift of λ_m.

Figure 3(b) shows clear interference fringes in the reflection spectra of the proposed HVILOFFP cavities. The FSRs of the reflection spectra were 12.5, 17.7, and 27.7 nm, and thus, the corresponding L values were approximately 94, 67, and 43 μm, respectively. To illustrate the experimental results, we simulated the normalized reflection spectra of the HVILOFFP cavities based on Eqs. (1) and (2) with $\alpha_1 = \alpha_2 = 0.001$, $n_{an} = 1$, $n_{co} = 1.46$, and $\gamma = 0.245, 0.117$, and 0.082
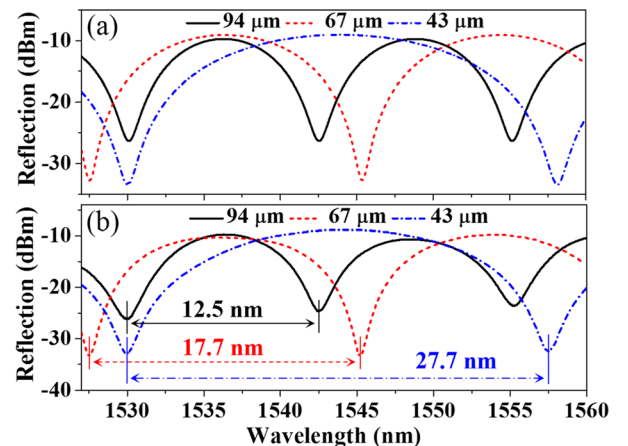

FIG. 3. (a) Simulated reflection spectra and (b) measured reflection spectra of the HVILOFFP cavities with cavity lengths of 94, 67, and 43 μm.

for the HVILOFFP cavities with $L = 94$, 67, and 43 μm, respectively, as shown in Fig. 3(a). The different γ values mainly result from the different mode-mismatch losses γ_2, where γ_2 increases as L increases, according to Eq. (4). Therefore, the fringe visibility of the HVILOFFP cavity can be improved by decreasing L. As shown in Figs. 3(a) and 3(b), the experimental results are consistent with the simulated spectra. The mode-mismatch loss of the HVILOFFP cavity is similar to that of the laser-machined FP cavities. However, the loss factors α_1 *and* α_2 at Mirrors 1 and 2 in the laser-machined FP cavities are more than those in the HVILOFFP cavity due to the rougher surfaces in laser-machined FP cavities. Moreover, rough mirrors in an FP cavity not only affect the fringe visibility but also decrease the intensity of the reflected light. The experimental results in Fig. 3(b) show that the fringe visibility of the HVILOFFP cavity with a 43-μm cavity length is up to 24.2 dB in air, which is higher than that of most laser-machined in-line FP cavities.

To demonstrate the HVILOFFP cavity, we tested the response of the proposed device to the RI by using refractive index matching liquids at room temperature. The HVILOFFP cavity was dipped in the analyte sample at an inclination of $\approx 5°$) between the liquid level and the axis of the fiber. Experiments showed that the analyte sample could smoothly flow into the HVILOFFP cavity through the two large holes in the sides of the HVILOFFP cavity without any assisting equipment (e.g., ultrasonic bath or syringe) to force the fluids. In our experiments, the HVILOFFP cavity was carefully cleaned with alcohol and was dried to eliminate the residual sample in the cavity until the reflection spectrum of the HVILOFFP cavity in air was recovered before each test. Figure 4(b) shows the response of the HVILOFFP cavity with $L = 94$ μm to analyte samples with different RIs from 1.333 to 1.339. Only several dozen femtoliters of the analyte sample were needed to completely fill the cavity to measure the RI. The dip
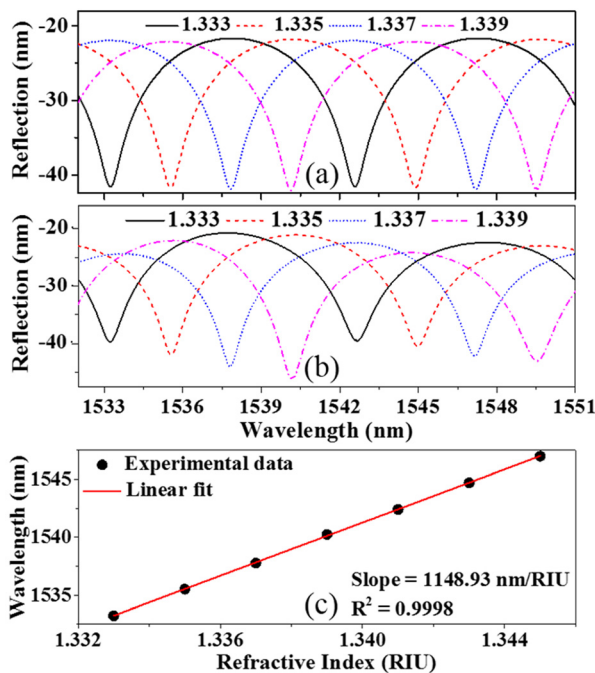

FIG. 4. (a) Simulated reflection spectra, (b) measured reflection spectra, and (c) dip wavelength evolution of the HVILOFFP cavity with different RIs (from 1.333 to 1.345).

wavelength of the reflection spectrum gradually shifted to the long wavelength region (redshift) as the RI of the analyte sample increased, which is consistent with the simulated data obtained with $\alpha_1 = \alpha_2 = 0.001$, $n_{co} = 1.46$, and $\gamma = 0.175$ in Fig. 4(a). The redshift of the dip wavelength is due to the increase in the optical path with the increase in the RI of the sample. In addition, the dip intensity of the reflection spectrum decreased from −39.6 dBm to −46.2 dBm when the RI of the analyte sample increased from 1.333 to 1.339. This can be explained as follows. According to Eq. (4), the mode-mismatch loss γ_2 is inversely proportional to n_{an}. The fringe visibility of the proposed two-beam FP cavity is maximum when the intensities of the beams are equal. In addition, the reflectivity of Mirror 1 is equal to that of Mirror 2 in this device. Therefore, the fringe visibility increases and the dip intensity decreases gradually as the RI n_{an} increases.

We traced the evolution of the dip wavelength (1533.23 nm) to analyze the RI sensitivity of the HVILOFFP cavity further. As shown in Fig. 4(c), the experimental data are fitted linearly and the RI sensitivity of the HVILOFFP cavity is 1148.93 nm/RIU in the range of 1.333–1.345. The measured RI sensitivity is close to the simulated value of 1150.20 nm/RIU from Eq. (6). Similar experimental results were observed for other HVILOFFP cavities with different L values.

The temperature response of the HVILOFFP cavity is similar to that reported in our previous work.[23] According to Eq. (6), the RI error of the cavity resulting from the thermal expansion of the SCT is as low as $7.49 \times 10^{-7}/°C$ (the thermal expansion coefficient of silica is $\sim 0.56 \times 10^{-6}/°C$). Thus, the proposed device is insensitive to ambient temperature.

In this work, we demonstrated an HVILOFFP cavity based on SCT and SMF. The optical FP cavity formed by the end faces of the two SMFs also functions as a microfluidic cavity, where two size-controllable microfluidic accesses were fabricated in the HVILOFFP cavity by polishing the latter SMF. Experimental results showed that the analyte sample could smoothly flow into the cavity and interact with light through the two accesses. The fringe visibility of the HVILOFFP cavity was higher than that of most laser-machined FP cavities because of the smoother mirrors in the SMFs. The proposed HVILOFFP cavity was demonstrated by measuring the RIs of analyte samples with a sensitivity of 1148.93 nm/RIU in the range of 1.333–1.345. Furthermore, the economical raw materials and simple fabrication process make the proposed device extremely low-cost. Therefore, this device is a promising candidate for applications in chemical and biomedical sensing because of its advantages like compact size (< 100 μm), insensitivity to temperature, simple fabrication, and mechanical robustness.

[1]D. Psaltis, S. R. Quake, and C. Yang, Nature **442**, 381 (2006).
[2]C. Monat, P. Domachuk, and B. J. Eggleton, Nat. Photonics **1**, 106 (2007).

[3]Y. Guo, H. Li, K. Reddy, H. S. Shelar, V. R. Nittoor, and X. Fan, Appl. Phys. Lett. **98**, 041104 (2011).

[4]J. Sadeghi, A. H. B. Ghasemi, and H. Latifi, Lab Chip **16**, 3957 (2016).

[5]M. Calcerrada, C. Garcia-Ruiz, and M. Gonzalez-Herraez, Laser Photonics Rev. **9**, 604 (2015).

[6]P. Vaiano, B. Carotenuto, M. Pisco, A. Ricciardi, G. Quero, M. Consales, A. Crescitelli, E. Esposito, and A. Cusano, Laser Photonics Rev. **10**, 922 (2016).

[7]Y. Wang, C. R. Liao, and D. N. Wang, Opt. Express **18**, 18056 (2010).

[8]W. Jin, Y. Cao, F. Yang, and H. L. Ho, Nat. Commun. **6**, 6767 (2015).

[9]C. Wu, M. L. V. Tse, Z. Liu, B. O. Guan, C. Lu, and H. Y. Tam, Opt. Lett. **38**, 3283 (2013).

[10]N. Zhang, G. Humbert, Z. Wu, K. Li, P. P. Shum, N. M. Y. Zhang, Y. Cui, J. Auguste, X. Q. Dinh, and L. Wei, Opt. Express **24**, 27674 (2016).

[11]Y. Ruan, E. P. Schartner, H. Ebendorff-Heidepriem, P. Hoffmann, and T. M. Monro, Opt. Express **15**, 17819 (2007).

[12]Z. He, Y. Zhu, and H. Du, Appl. Phys. Lett. **92**, 044105 (2008).

[13]G. Emiliyanov, P. E. Hoiby, L. H. Pedersen, and O. Bang, Sensors **13**, 3242 (2013).

[14]M. S. Cheri, H. Shahraki, J. Sadeghi, M. S. Moghaddam, and H. Latifi, Biomicrofluidics **8**, 054123 (2014).

[15]M. S. Cheri, H. Latifi, J. Sadeghi, M. S. Moghaddam, H. Shahraki, and H. Hajghassem, Analyst **139**, 431 (2014).

[16]Q. Zhang, X. Tian, P. Hao, Z. Li, X. Wang, and Y. Li, "High-visibility in-fiber open-cavity Fabry–Pérot optofluidic sensor based on a suspended-core fiber," (submitted).

[17]Y. Rao, M. Deng, D. Duan, X. Yang, T. Zhu, and G. Cheng, Opt. Express **15**, 14123 (2007).

[18]C. R. Liao, T. Y. Hu, and D. N. Wang, Opt. Express **20**, 22813 (2012).

[19]L. Yuan, J. Huang, X. Lan, H. Wang, L. Jiang, and H. Xiao, Opt. Lett. **39**, 2358 (2014).

[20]C. Ma and A. Wang, Opt. Lett. **35**, 2043 (2010).

[21]J. Li, F. Albri, R. R. J. Maier, W. Shu, J. Sun, D. P. Hand, and W. N. MacPherson, IEEE Sens. J. **15**, 7221 (2015).

[22]K. B. Gavan, J. H. Rector, K. Heeck, D. Chavan, G. Gruca, T. H. Oosterkamp, and D. Iannuzzi, Opt. Lett. **36**, 2898 (2011).

[23]Q. Zhang, T. Zhu, Y. Hou, and K. S. Chiang, J. Opt. Soc. Am. B **30**, 1211 (2013).